Title: Novel Scalable MIMO Channel Sounding Technique and Measurement Accuracy Evaluation with Transceiver Impairments

Authors: Minseok Kim, Jun-ichi Takada, and Yohei Konishi

Affiliations: Graduate School of Science and Engineering, Tokyo Institute of Technology, Japan

Published in: IEEE Transactions on Instrumentation and Measurement, Vol.61, No.12, pp. 3185–3197, Dec. 2012

DOI: 10.1109/TIM.2012.2205510

Novel Scalable MIMO Channel Sounding Technique and Measurement Accuracy Evaluation with Transceiver Impairments

Minseok Kim, *Member, IEEE,* Jun-ichi Takada, *Senior Member, IEEE,* and Yohei Konishi, *Student Member, IEEE,*

***Abstract*—This paper presents a novel MIMO channel sounding technique with a fully parallel transceiver architecture that employs a layered scheme of frequency and space-time division multiplexing. It offers inherent scalability of the number of antennas by a combination of multiple transceiver units and flexibility for both directional MIMO channel and multi-link MIMO channel measurements. This paper describes the principle of the channel sounding technique and formulates the signal processing that makes possible various scalable unit configurations. The influence of the transceiver imperfections such as I/Q imbalance (IQI) and phase noise (PN) on the measurement accuracy is discussed, and a multitone allocation scheme that is robust against IQI is also introduced. Using computer simulations, the measurement accuracy in the presence of IQI and PN is evaluated using the normalized mean square error, which provides a design guideline for the realization of hardware.**

***Index Terms*—Channel sounding, MIMO, Frequency division multiplexing, Scalability, Fully parallel architecture, Directional channel, Multi-link MIMO channel**

I. Introduction

Knowledge of the radio channel property is usually necessary for developing wireless transmission systems. In future cellular systems with MIMO (multiple-input-multiple-output) technology, it will become necessary to operate in a smaller cellular environment than before to increase the capacity to a much greater degree where the channel behaviors are quite specific to the individual environments. In particular, the design and analysis of multi-link technologies such as multi-user MIMO (MU-MIMO) and base station cooperation require more sophisticated channel models of correlation among the links and the ranks of the channels. In addition, it is also necessary to investigate the details of the directional properties of the environment for predicting the possible channel ranks and for designing MIMO array antennas.

So far, channel sounders have conventionally been designed for point-to-point measurement. However, the increasing demand for multi-link channel characterization requires a scalable channel sounding architecture that is suitable for flexible measurement configurations and robust against various practical issues on distributed systems. A response to the challenge to utilize two heterogeneous channel sounders for dual-link MIMO channel characterization was presented in [1], [2], but it suffered from a few practical problems such as synchronization between two different systems. MU-MIMO measurements with a single sounder by separation of the array antennas have been conducted in very limited measurement scenarios [3], [4]. To meet the above demands, a scalable channel sounding architecture and an efficient signal processing technique are desirable.

The authors are with Graduate School of Science and Engineering, Tokyo Institute of Technology, Tokyo, Japan (e-mail:mskim@ieee.org).

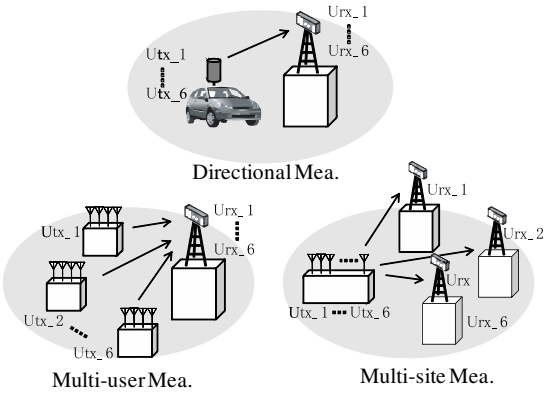

Fig. 1. Various measurement configurations with scalable architecture (with up to six units).

With regard to the channel sounding techniques, various methods have been developed for characterizing a radio channel property, including pulse sounding, frequency sweep, and cross-correlation using a known sounding signal. For MIMO channel sounding, multiplexing techniques would be necessary for separating all the transmitted signals from multiple antennas; thus, individual channel responses can be obtained on the receiver side. Basically, TDM (time division multiplexing) [5]–[8], FDM (frequency division multiplexing) [9], [10], and CDM (code division multiplexing) [11], [12] schemes can be chosen appropriately, or a hybrid method among them can be applied according to the system architecture. The advantages and drawbacks of these approaches have already been well discussed in the literature, e.g., [13].

In developing channel sounders, many design and implementation issues must be practically considered. As previously discussed well in many published research works, the measurement accuracy of channel sounders is limited by various hardware imperfections as the transmission performance of wireless transceivers degrades. Such imperfections including the ADCs'/DACs' phase, gain, and offset mismatch [14], the RF transceiver's carrier leakage, I/Q mismatch [6], [14]–[18], and nonlinearity [14], local oscillator (LO) phase noise and frequency error [14], [20]–[23], among others. It is therefore

necessary to understand these imperfections to develop channel sounders properly. However, to the best of our knowledge, there has yet to be any comprehensive discussion on the design and implementation issues involved in developing channel sounders.

A. Overview of Channel Sounder Architectures

For MIMO channel measurement, a fully switching architecture that has a single radio front-end at both sides of the transmitter and receiver has been widely accepted [5]–[8]; an example of this is the RUSK MIMO channel sounder by MEDAV [5]. The advantages of such an architecture include the low complexity of signal processing, simplicity of RF calibration, easy cabling to the antenna, and a relatively low development cost per channel. On the other hand, the following drawbacks are also well known. First, the number of antennas to be switched usually limits the channel acquisition rates, making it difficult to measure the high Doppler frequency in some dynamic environments. As a tradeoff, the measurement delay spread is also limited. Second, such an architecture suffers from large switching loss and a spatially distributed phase noise effect [23].

In order to reduce the measurement duration, a transmitter switching architecture that has a single radio front-end at the transmitter but a complete set at the receiver [24], and a fully parallel architecture that has complete sets of radio front-ends at both the transmitter and receiver [10], [25] have been considered. These architectures can reduce the measurement duration per snapshot by $1/N_{\mathrm{R}}$, where N_{R} denotes the number of receive antennas. Although a fully parallel architecture is also free of transmit switching, unfortunately, it cannot reduce the measurement duration any further because simultaneous transmission requires a repetitive transmission of the original signal or long symbol duration for the number of signals to be transmitted simultaneously for signal separation on the receiver side. As mentioned above, a long measurement duration limits measurement capability of Doppler characteristics in dynamic environments and leads to measurement errors from the phase noise effect. However, it should be noted that an additional gain in the SNR (signal-to-noise power ratio) at the receiver side can be achieved thanks to the simultaneous repetitive transmission.

In this paper, a novel architecture based on a modular concept of a transmitter and receiver unit is proposed. It offers an easy extension with new units, combination with multiple units for directional MIMO channel measurement, and spatial separation into multiple units for multi-link MIMO measurement, as shown in Fig.1. The FDM and STDM (space-time division multiplexing) layered scheme allows simultaneous repetitive transmission for all transmit antennas, which in turns offers a certain processing gain in SNR. As a result, the transmission power per transmit antenna can be regulated and maintained relatively small. Moreover, it is also beneficial in that the same hardware can be utilized for both MIMO transmission evaluation and propagation channel measurement simultaneously.

B. Contributions

The original contributions of this paper are as follows.

- In Section II, this paper proposes a novel scalable channel sounding concept for making flexible measurements in various scenarios, which is promising for the characterization of radio channels in future wireless systems. With its inherent scalability, it is suitable for both directional MIMO channel and multi-link MIMO channel measurements. Moreover, a signal processing technique of MIMO multiplexing involving a novel FDM-STDM layered scheme on a fully parallel transceiver architecture is proposed.
- Using normalized mean square error (NMSE) as a figure of merit for the measurement accuracy evaluation, the design and implementation criteria are comprehensively discussed from the point of view of channel sounding, in Section III.
- A multitone allocation scheme that is robust against IQI and that can greatly relax the requirement of the transceiver I/Q imbalance (IQI) compensation is proposed in Section IV-A.
- The channel measurement accuracy is evaluated in terms of various scalable configurations in the presence of the most critical impairments of the RF front-ends, IQI and phase noise (PN) by using computer simulations, in Section V.

II. Channel Sounding Principle

Consider $N_{\mathrm{T}} \times N_{\mathrm{R}}$ MIMO channel sounding with N_{Utx} transmitter units, each of which has L transmit antennas, where $N_{\mathrm{T}} = N_{\mathrm{Utx}}L$, and likewise with N_{Urx} receiver units where $N_{\mathrm{R}} = N_{\mathrm{Urx}}L$. In this paper, a layered scheme using FDM and STDM is developed to multiplex the transmitting signals from N_{T} antennas. In this paper, the sounding principle is formulated by equivalent complex lowpass representation.

A. Notations

$s[n']$:	oversampled symbol
$s^{((l))}[n'']$:	l-th FDM symbol
$\bar{s}^{((l))}[i]$:	l-th FDM symbol with GI (guard interval)
$\boldsymbol{x}^{((l),m)}[i]$:	l-th FDM transmit signal vector in m-th STDM slot
$\boldsymbol{x}^{(m)}[i]$:	Transmit signal vector in m-th STDM slot
$\boldsymbol{X}^{(m)}[k'']$:	Transmit multitone vector in m-th STDM slot
$\boldsymbol{X}^{((l),m)}[k]$:	l-th FDM transmit multitone vector in m-th STDM slot
$\boldsymbol{X}^{((l))}[k]$:	l-th FDM transmit multitone matrix
$\boldsymbol{y}^{(m)}[i]$:	Receive signal vector in m-th STDM slot
$\boldsymbol{Y}^{(m)}[k'']$:	Receive multitone vector in m-th STDM slot
$\boldsymbol{Y}^{((l),m)}[k]$:	l-th FDM receive multitone vector in m-th STDM slot
$\boldsymbol{Y}^{((l))}[k]$:	l-th FDM receive multitone matrix
$\boldsymbol{z}^{(m)}[i]$:	Noise signal vector in m-th STDM slot
$\boldsymbol{Z}^{(m)}[k'']$:	Noise response vector in m-th STDM slot
$\boldsymbol{Z}^{((l),m)}[k]$:	l-th FDM noise response vector in m-th STDM slot
$\boldsymbol{Z}^{((l))}[k]$:	l-th FDM noise response matrix

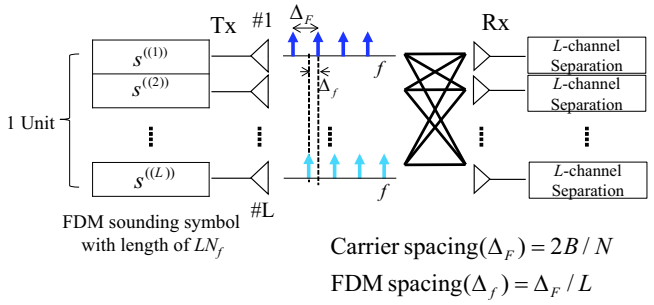

Fig. 2. L channel FDM channel sounding scheme with a multitone signal where $\Delta_f = \Delta_F/L$.

$\boldsymbol{h}[\tau]$: Channel impulse response matrix
$\boldsymbol{H}[k'']$: Channel transfer function matrix
$\boldsymbol{H}^{((l))}[k]$: l-th FDM channel transfer function matrix
where
N: Number of tones
N_f: FFT length
N_{GI}: GI length
N_s: Symbol length ($N_{\mathrm{GI}} + N_f$)
n': Oversampled symbol sample index $(0, \cdots, N_f - 1)$
n'': FDM symbol sample index $(0, \cdots, LN_f - 1)$
i: FDM symbol sample index (with GI) $(0, \cdots, LN_s - 1)$
k: Multitone index $(0, \cdots, N - 1)$
k': Oversampled multitone index $(0, \cdots, N_f - 1)$
k'': FDM multitone index $(0, \cdots, LN - 1)$

B. Multiplexing for Multiple Signals within the Same Transmitter Unit

Consider the FDM for the transmitting signals within the same transmitter unit as shown in Fig. 2. The sounding signal for the l-th FDM channel is represented by

$$s^{((l))}(t) = s(t)\exp\left(\mathrm{j}2\pi(l-1)\Delta_f t\right) \text{ for } l = 1, ..., L, \quad (1)$$

which indicates the frequency shifted version of $s(t)$. In (1), we consider the unmodulated complex Newman phase multitone (NPM) signal

$$s(t) = \frac{1}{\sqrt{N}} \sum_{k=-N/2}^{N/2-1} \exp\left(\mathrm{j}2\pi k\Delta_F t + \mathrm{j}\phi_k\right) \quad (2)$$

with Newman phases $\phi_k = \frac{k^2\pi}{N}$ for peak-to-average power ratio (PAPR) reduction [26]. Here, N denotes the number of sub-carriers (tones) to be allocated over the given frequency band $2B$, Δ_F denotes the sub-carrier spacing and the FDM frequency shift $\Delta_f = \Delta_F/L$ [9]. Using the relation $\Delta_F = 2B/N$, the discrete time representation of (1), assuming a sampling rate $f_s = 2BR_{\mathrm{ov}}$ (R_{ov} denotes the over-sampling ratio of the sampling rate to the bandwidth), is expressed as

$$s^{((l))}[n''] = s[\mathrm{mod}\,(n'', N_f)]\exp\left(\mathrm{j}\frac{2\pi(l-1)n''}{LN_f}\right) \quad (3)$$

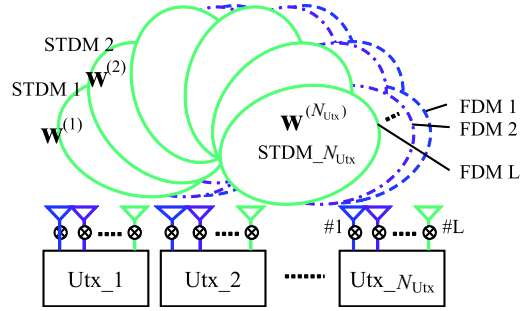

(a) FDM-STDM layered multiplexing scheme.

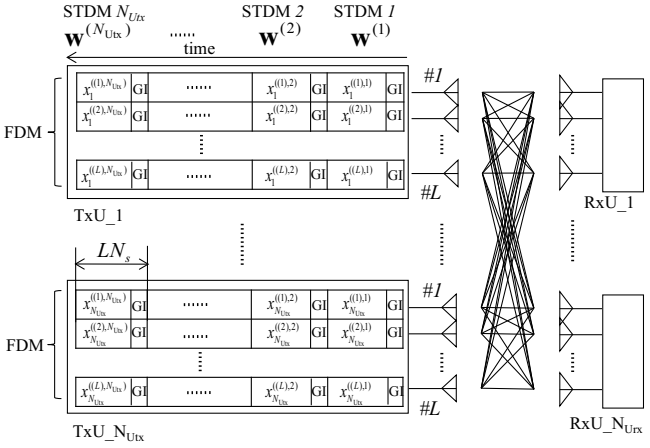

(b) Sounding frame format.

Fig. 3. Multiplexing for scalable MIMO channel sounding.

for $n'' = 0, ..., LN_f - 1$, where $\mathrm{mod}(a, b)$ denotes the remainder upon the division of a by b, $N_f = R_{\mathrm{ov}}N$, and

$$s[n'] = \frac{1}{\sqrt{N_f}} \sum_{k'=0}^{N_f-1} \bar{\Psi}_{k'} \exp\left(\mathrm{j}\frac{2\pi}{N_f}k'n'\right) \quad (4)$$

for $n' = 0, ..., N_f - 1$. The interpolated NPM sequence in frequency domain

$$\bar{\Psi}_{k'} = \begin{cases} \sqrt{R_{\mathrm{ov}}}\Psi_{k'} & 0 \le k' < \frac{N}{2} \\ \sqrt{R_{\mathrm{ov}}}\Psi_{N-N_f+k'} & N_f - \frac{N}{2} \le k' < N_f \\ 0 & \text{otherwise} \end{cases}, \quad (5)$$

where $\Psi_k = \exp(\mathrm{j}\phi_k)$. (4) can be calculated by N_f-point inverse fast Fourier transform (IFFT). As shown in Fig. 2 it is noted that the measurement duration for the L channel FDM becomes L times longer than that for a single channel.

C. Multiplexing for Multiple Signals among Multiple Transmitter Units

Fig. 3(a) shows the concept of the FDM-STDM layered multiplexing scheme with N_{Utx} transmitter units, each of which has L transmit antennas. To multiplex transmitting signals from multiple transmitter units, a scalable data frame

structure with multiple STDM symbol slots-the same number of slots as there are transmitter units ($m = 1, ..., N_{\mathrm{Utx}}$)-is introduced.

By aggregating the transmitting signals at the antenna elements corresponding to the l-th FDM channel in each unit, the transmitting signal vector in the m-th STDM slot is written as

$$\begin{aligned} \boldsymbol{x}^{((l),m)}[i] &= \begin{bmatrix} x_l[i+(m-1)LN_s] \\ x_{L+l}[i+(m-1)LN_s] \\ \vdots \\ x_{L(N_{\mathrm{Utx}}-1)+l}[i+(m-1)LN_s] \end{bmatrix} \\ &= \sqrt{N_{\mathrm{Utx}}}\boldsymbol{w}^{(m)}\bar{s}^{((l))}[i], \end{aligned} \tag{6}$$

for $i = 0, ..., LN_s - 1$, $N_s = N_f + N_{\mathrm{GI}}$ where x_u and N_{GI} denote the signal transmitted at u-th antenna ($u = 1, ..., N_{\mathrm{T}}$) and the length of GI (guard interval) that is added as a cyclic prefix, respectively. It should be noted that the sounding symbols are different in every STDM slot; thus, the cyclic prefix should be inserted by copying the last N_{GI} samples into the top of each symbol to maintain the orthogonality among the STDM channels, even in the reception of delayed signals. In this scheme, the delay spread to be measured is determined by the duration of the GI. $\boldsymbol{w}^{(m)} \in \mathbb{C}^{N_{\mathrm{Utx}}\times 1}$ is a transmit orthogonal beamforming weight vector for the m-th STDM slot with unit gain. For the beamforming weight vectors, the DFT (discrete Fourier transform) beams can be used where the p-th element for m-th STDM slot is written as

$$w_p^{(m)} = \frac{1}{\sqrt{N_{\mathrm{Utx}}}} \exp\left(\mathrm{j}\frac{2\pi(m-1)(p-1)}{N_{\mathrm{Utx}}}\right) \tag{7}$$

for $p = 1, ..., N_{\mathrm{Utx}}$. Also,

$$\bar{s}^{((l))}[i] = \bar{s}^{((1))}[i] \exp\left(\mathrm{j}\frac{2\pi(l-1)i}{LN_f}\right), \tag{8}$$

where the sounding signal with a cyclic prefix for the l-th FDM channel based on (4) is rewritten as

$$\bar{s}^{((1))}[i] = \frac{1}{\sqrt{LN_f}} \sum_{n''=0}^{LN_f-1} \tilde{\Psi}_{n''} \exp\left(\mathrm{j}\frac{2\pi}{LN_f} n''\left(i - LN_{\mathrm{GI}}\right)\right), \tag{9}$$

where

$$\tilde{\Psi}_{n''} = \begin{cases} \sqrt{L}\bar{\Psi}_{\frac{n''}{L}} & \mathrm{mod}(n'', L) = 0 \\ 0 & \text{otherwise} \end{cases}. \tag{10}$$

It is noted that in (6), the signal is multiplied by $\sqrt{N_{\mathrm{Utx}}}$ to maintain the transmitting power per antenna (phase control only). As shown in Fig. 3(b), the signal for each FDM channel at the m-th STDM slot, which is generated by (6), is simultaneously transmitted in multiple time slots by transmitting beamforming. Since the transmitting power is usually limited within a certain level, the SNR per transmit antenna for each MIMO channel can be improved by transmit beamforming, which is called an *STDM gain* of N_{Utx} times.

At the receiver side, the received signal vector in the m-th STDM slot can be represented as

$$\boldsymbol{y}^{(m)}[i] = \sum_{\tau=0}^{LN_{\mathrm{GI}}-1} \boldsymbol{h}[\tau]\boldsymbol{x}^{(m)}[i-\tau] + \boldsymbol{z}^{(m)}[i], \tag{11}$$

where $\boldsymbol{h}[\tau] \in \mathbb{C}^{N_{\mathrm{R}}\times N_{\mathrm{T}}}$ denotes the MIMO channel impulse response matrix, $\boldsymbol{z}^{(m)}[i]$ is a complex additive white Gaussian noise process with a power of P_z ($E[\boldsymbol{z}\boldsymbol{z}^H] = P_z\boldsymbol{I}$),

$$\boldsymbol{x}^{(m)}[i] = \begin{bmatrix} x_1[i+(m-1)LN_s] \\ \vdots \\ x_{N_{\mathrm{T}}}[i+(m-1)LN_s] \end{bmatrix}, \tag{12}$$

$$\boldsymbol{y}^{(m)}[i] = \begin{bmatrix} y_1[i+(m-1)LN_s] \\ \vdots \\ y_{N_{\mathrm{R}}}[i+(m-1)LN_s] \end{bmatrix}, \tag{13}$$

$$\boldsymbol{z}^{(m)}[i] = \begin{bmatrix} z_1[i+(m-1)LN_s] \\ \vdots \\ z_{N_{\mathrm{R}}}[i+(m-1)LN_s] \end{bmatrix}, \tag{14}$$

where y_v and z_v denote the received signal and noise at the v-th antenna ($v = 1, ..., N_{\mathrm{R}}$), respectively. After removal of the cyclic prefix, (11) is converted into the frequency domain by DFT. By extracting only the signal band at a lower frequency from the oversampled signal spectrum, we obtain

$$\boldsymbol{Y}^{(m)}[k''] = \boldsymbol{H}[k'']\boldsymbol{X}^{(m)}[k''] + \boldsymbol{Z}^{(m)}[k''] \tag{15}$$

for $k'' = 0, ..., LN - 1$. Consider the l-th FDM channel in (15) as

$$\boldsymbol{Y}^{((l),m)}[k] = \boldsymbol{H}^{((l))}[k]\boldsymbol{X}^{((l),m)}[k] + \boldsymbol{Z}^{((l),m)}[k] \tag{16}$$

where

$$\boldsymbol{X}^{((l),m)}[k] = \boldsymbol{X}^{(m)}[Lk+l], \tag{17}$$

$$\boldsymbol{Y}^{((l),m)}[k] = \boldsymbol{Y}^{(m)}[Lk+l], \tag{18}$$

$$\boldsymbol{Z}^{((l),m)}[k] = \boldsymbol{Z}^{(m)}[Lk+l], \tag{19}$$

for $k = 0, ..., N-1$, which indicates the sub-carrier selection corresponding to the l-th FDM channel. It should be noted that the output SNR for each MIMO channel increases by L times; this is called the *FDM gain*.

In this paper, we assume a time-invariant channel across the duration of all STDM slots. That is to say,

$$\begin{aligned} \boldsymbol{Y}^{((l),1)}[k] &= \boldsymbol{H}^{((l))}[k]\boldsymbol{X}^{((l),1)}[k] + \boldsymbol{Z}^{((l),1)}[k], \\ &\vdots \\ \boldsymbol{Y}^{((l),N_{\mathrm{Utx}})}[k] &= \boldsymbol{H}^{((l))}[k]\boldsymbol{X}^{((l),N_{\mathrm{Utx}})}[k] + \boldsymbol{Z}^{((l),N_{\mathrm{Utx}})}[k]. \end{aligned}$$

Therefore, it can be rewritten as

$$\boldsymbol{Y}^{((l))}[k] = \boldsymbol{H}^{((l))}[k]\boldsymbol{X}^{((l))}[k] + \boldsymbol{Z}^{((l))}[k] \tag{20}$$

where

$$\boldsymbol{X}^{((l))}[k] = \begin{bmatrix} \boldsymbol{X}^{((l),1)}[k] & \cdots & \boldsymbol{X}^{((l),N_{\mathrm{Utx}})}[k] \end{bmatrix} \in \mathbb{C}^{N_{\mathrm{Utx}}\times N_{\mathrm{Utx}}}, \tag{21}$$

$$\boldsymbol{Y}^{((l))}[k] = \left[\begin{array}{ccc} \boldsymbol{Y}^{((l),1)}[k] & \cdots & \boldsymbol{Y}^{((l),N_{\mathrm{Utx}})}[k] \end{array} \right] \in \mathbb{C}^{N_{\mathrm{R}} \times N_{\mathrm{Utx}}}, \quad (22)$$

$$\boldsymbol{Z}^{((l))}[k] = \left[\begin{array}{ccc} \boldsymbol{Z}^{((l),1)}[k] & \cdots & \boldsymbol{Z}^{((l),N_{\mathrm{Utx}})}[k] \end{array} \right] \in \mathbb{C}^{N_{\mathrm{R}} \times N_{\mathrm{Utx}}}, \quad (23)$$

$$\boldsymbol{H}^{((l))}[k] = \left[\begin{array}{ccc} \boldsymbol{H}_l[k] & \cdots & \boldsymbol{H}_{L(N_{\mathrm{Utx}}-1)+l}[k] \end{array} \right] \in \mathbb{C}^{N_{\mathrm{R}} \times N_{\mathrm{Utx}}}, \quad (24)$$

$$\boldsymbol{W} = \left[\begin{array}{ccc} \boldsymbol{w}^{(1)} & \cdots & \boldsymbol{w}^{(N_{\mathrm{Utx}})} \end{array} \right] \in \mathbb{C}^{N_{\mathrm{Utx}} \times N_{\mathrm{Utx}}}, \quad (25)$$

and $\boldsymbol{H}_l$ denotes the l-th column vector of $\boldsymbol{H}$. From the relations of (5), (6) and (10), the l-th FDM transmit multitone vector in the m-th STDM slot in (17) can be rewritten as

$$\boldsymbol{X}^{((l),m)}[k] = \boldsymbol{w}^{(m)} \sqrt{LR_{\mathrm{ov}} N_{\mathrm{Utx}}} \Psi_k \quad (26)$$

which is in fact the DFT of the down-sampled and cyclic prefix removed version of (6). It should also be noted that the right-hand term of (26) is independent of FDM channel l and that the frequency shifted versions of the same multitone Ψ_k are transmitted. However, each l covers different sub-carriers as shown in Fig.2. Consequently by substituting (26) into (21), (20) can be rewritten as

$$\boldsymbol{Y}^{((l))}[k] = \boldsymbol{H}^{((l))}[k] \boldsymbol{W} \left(\sqrt{LR_{\mathrm{ov}} N_{\mathrm{Utx}}} v \Psi_k \right) + \boldsymbol{Z}^{((l))}[k]. \quad (27)$$

By dividing (27) with $\boldsymbol{W} \left(\sqrt{LR_{\mathrm{ov}} N_{\mathrm{Utx}}} \Psi_k \right)$, the matrix of the MIMO channel transfer function for the l-th FDM channel is finally obtained by

$$\hat{\boldsymbol{H}}^{((l))}[k] = \boldsymbol{H}^{((l))}[k] + \boldsymbol{Z}^{((l))}[k] \left(\sqrt{LR_{\mathrm{ov}} N_{\mathrm{Utx}}} \Psi_k \right)^{-1} \boldsymbol{W}^{-1}. \quad (28)$$

Using (28), the transfer functions for all FDM channels can be calculated separately and hence $\hat{\boldsymbol{H}}[k] \in \mathbb{C}^{N_{\mathrm{R}} \times N_{\mathrm{T}}}$ is obtained. As can be seen from (28), the channel measurement accuracy increases with a large path gain that maintains the received signal power at a level that is sufficiently greater than the receiver noise floor. To cope with the influence of noise, channel sounders can increase the SNR by taking the average of the snapshots for consecutive sounding symbols, as long as the channel can be maintained as being static.

III. Measurement Accuracy and Performance Metric

In developing a channel measurement system, the measurement accuracy should be clearly analyzed, because the system will be implemented based upon design criteria to meet a given required performance. It is obvious that to achieve a better radio propagation channel analysis, accurate channel measurement is indispensable, but the impairment of circuits and the limited precision of components actually degrade the measurement accuracy. Hence, the design criteria need to be introduced to determine the compensation level of the circuit impairments and the selection of components.

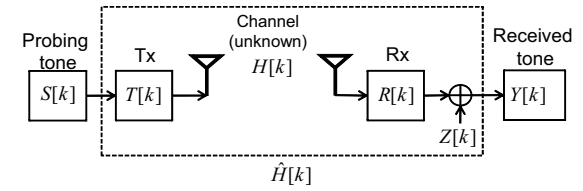

(a) Channel measurement.

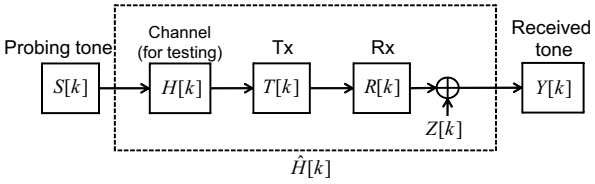

(b) Testing measurement for transceiver compensation and calibration.

Fig. 4. Block diagrams of channel measurement and transceiver testing processes.

Although the purpose of a channel sounder is not data transmission, design criteria similar to those of wireless transmission systems can be considered simply because they have basically the same architecture. However, unlike data-centric figures of merit such as EVM (error vector magnitude) and BER (bit error rate) in the designing and testing of wireless transmission systems, those used for designing channel sounders have not been comprehensively investigated. The reason for this is that the radio channel measured by channel sounders is further utilized for other purposes, while the quality of the received data directly determines the performance of the transmission system, and hence, EVM and BER can be insightful performance metrics.

A. Transceiver Testing for Channel Sounders

Fig. 4(a) shows a simplified channel measurement process in a frequency domain for the k-th probing tone $S[k]$, where $Y[k]$ denotes the received tone, $H[k]$ denotes the unknown channel to be measured, and $T[k]$ and $R[k]$ denote the responses of the transmitter and receiver, respectively. $Z[k]$ denotes an additive Gaussian noise process. The transceiver imperfections indicate the impact of the impairments of the circuits and the limited precision of components, which must be compensated for and carefully determined for accurate measurement, as will be discussed further in Section IV.

The frequency characteristics of the components are usually calibrated by the measured responses in a direct cable connection between the transmitter and receiver antenna ports, which is called *back-to-back calibration*. Consequently, the channel transfer function can be estimated. However, the channel estimation accuracy will be degraded if the hardware imperfections are included in the measured channel. In general, transceiver imperfections can only be observed as mixed characteristics and are not separable from the frequency

characteristics of the transmitter and receiver. However, we assume that they are ideally calibrated, or $R[k]T[k] = 1, \forall k$, and hence, only the transceiver imperfections are included in the measured channel $\hat{H}[k]$. In reality, we can determine the compensation level of the circuit impairments and the selection of components by evaluating their effects using mathematical analysis and computer simulations.

For transceiver testing prior to the radio channel measurement, consider a SISO (single-input-single-output) test measurement performed with the direct cable connection of a single transmitter and a single receiver, as shown in Fig. 4(b), to assess the practical measurement accuracy with a given transceiver, where $H[k]$ denotes a known channel response for testing. The channel estimation error $\left|\hat{H}[k] - H[k]\right|$ should be reduced in accordance with any specific design criteria. In Fig. 4(b), NMSE is defined as

$$\text{NMSE} = \frac{\sum_k \left|\hat{H}[k] - H[k]\right|^2}{\sum_k |H[k]|^2} \tag{29}$$

where

$$\begin{aligned} \hat{H}[k] &= Y[k]S^{-1}[k] \\ &= \eta[k]R[k]T[k]H[k] + Z[k]S^{-1}[k], \end{aligned} \tag{30}$$

and $\eta[k]$ represents multiplicative impairments due to IQI and PN. Therefore, (29) can be rewritten as

$$\text{NMSE} = \frac{\sum_k \left|(\eta[k]R[k]T[k] - 1)H[k] + Z[k]S^{-1}[k]\right|^2}{\sum_k |H[k]|^2}, \tag{31}$$

where $|S[k]| = 1$ (equal gain across the bandwidth). It is obvious that (31) is reduced to $1/\text{SNR}$ when $Z[k]$ is dominant over multiplicative impairments (or $\eta[k] \approx 1, \forall k$) and the frequency characteristics of transmitter and receiver ($T[k]$ and $R[k]$) are known to be eliminated from (31).

On the other hand, consider the EVM in transceiver testing for multi-carrier transmission systems such as OFDM (orthogonal frequency division multiplexing) in the same configuration as that shown in Fig. 4(b). The EVM is one of the widely used figures of merit used in the evaluation of the quality of transmission systems [27]; it is defined as

$$\text{EVM} = \sqrt{\frac{\sum_k \left|\hat{S}[k] - S[k]\right|^2}{\sum_k |S[k]|^2}} \tag{32}$$

where

$$\begin{aligned} \hat{S}[k] &= Y[k]\hat{H}^{-1}[k] \\ &= \xi[k]S[k] + Z[k]\hat{H}^{-1}[k], \end{aligned} \tag{33}$$

by signal detection with the estimated channel. Similar to the NMSE, (32) can be rewritten as

$$\text{EVM} = \sqrt{\frac{\sum_k \left|(\xi[k] - 1)S[k] + Z[k]\hat{H}^{-1}[k]\right|^2}{\sum_k |S[k]|^2}}. \tag{34}$$

If $\hat{H}[k] = R[k]T[k]H[k]$ (perfect channel estimation), $\xi[k]$ simply indicates $\eta[k]$ in (34). It can be seen that both (31) and (34) equivalently represent the effect of the multiplicative impairments with respect to the average path gain and the average signal power, respectively, when $T[k]$ and $R[k]$ are known and SNR is sufficiently large. This implies that the NMSE can be an appropriate performance metric for testing a non-data-centric instrumental system such as a channel sounder without modulation/demodulation and has a similar meaning of the $(\text{EVM})^2$ in transceiver testing. For example, the NMSE of 9.0×10^{-4} roughly corresponds to an EVM of 3%, which is a reasonable figure for a transceiver's performance.

B. MIMO Channel Sounding Accuracy

To evaluate the channel measurement accuracy of a MIMO channel sounder, the NMSE of the estimated transfer function to a known testing channel can be expressed by

$$\text{NMSE} = \frac{\sum_k \|\hat{\boldsymbol{H}}[k] - \boldsymbol{H}[k]\|_{\text{F}}^2}{\sum_k \|\boldsymbol{H}[k]\|_{\text{F}}^2}, \tag{35}$$

where the Frobenius norm $\|\boldsymbol{A}\|_{\text{F}} = \sqrt{\text{tr}(\boldsymbol{A}\boldsymbol{A}^H)}$. Using (28), which does not include transceiver imperfections, (35) can be rewritten as

$$\begin{aligned} \text{NMSE} &= \frac{N_{\text{T}}N_{\text{R}}N}{LR_{\text{ov}}N_{\text{Utx}}\left(P_s/P_z\right)\sum_k \|\boldsymbol{H}[k]\|_{\text{F}}^2} \\ &= \frac{1}{LR_{\text{ov}}N_{\text{Utx}} \cdot \gamma_0}, \end{aligned} \tag{36}$$

where $\gamma_0 = \frac{P_s}{P_z} \cdot \frac{1}{N_{\text{T}}N_{\text{R}}N} \sum_k \|\boldsymbol{H}[k]\|_{\text{F}}^2$ indicates the average SNR per transmit antenna and $P_{\text{s}} = E[|\Psi_k|^2]$. Hence, (36) implies that the NMSE is equivalent to the reciprocal of the average output SNR per transmit antenna over all MIMO channels. As discussed above, hardware imperfections further degrade the measurement accuracy.

IV. Effects of Transceiver Imperfections

In such a fully parallel MIMO transceiver architecture, many types of synchronization between multiple channels should be the most difficult and time-consuming task, because of the huge number of MIMO channels which exist as many as the product of the numbers of transmit and receive antennas. In the baseband processing part, the amplitude differences and phase skews among all ADCs and DACs within a certain unit and among units should be guaranteed. To be exact, at least, the I/Q skew should be precisely adjusted, even though the skews between channels can be eliminated by back-to-back calibrations. Moreover, the sampling and carrier frequency of the signal across different units should ideally be synchronized, which is usually realized by using a very high-precision atomic clock reference at every unit.

Although the baseband processing part and frequency synchronization are assumed to be perfect, the measurement accuracy is significantly degraded in the presence of transceiver impairments, which include the IQI in the quadrature modulators/demodulators, the phase noise of the local oscillators (LOs), the nonlinearity of the components, and so forth. This section discusses the two effects of IQI and PN on the channel measurement accuracy in the proposed sounding architecture,

since they are the most critical problems in the development of a wireless transceiver.

A. I/Q Imbalance (IQI) Effect and Multitone Allocation

In a super-heterodyne transceiver, the quadrature modulator/demodulator is generally realized in an analog circuit; thus, it usually suffers from in-phase quadrature (I/Q) imbalance, namely, gain difference and phase skew in the quadrature LO branches and DC offsets in the I/Q branches. These must be sufficiently compensated for because they cause mirror image distortion and generate carrier leakage. Many techniques that employ digital signal processing have been developed to compensate for these impairments [15]–[17].

In the proposed sounding scheme, the phase imbalance and amplitude difference between quadrature local oscillator branches [15], [18] generates interferences between FDM channels. Fig. 5(a) illustrates the frequency spectrum with full-tone allocation with N sub-carriers when $L = 4$. As can be seen, the image components of the FDM CH1 ($l = 1$) and CH3 ($l = 3$) interfere with the mirror sub-carriers of the same FDM channel, and CH2 ($l = 2$) and CH4 ($l = 4$) mutually interfere with each other. That leads to channel measurement error, which is classified as a deterministic error in a specific system, and can thus be effectively compensated for by digital signal processing [15]–[17].

Extending (29) to the case of MIMO case, (35) can be rewritten. Even if self- or inter-FDM-channel interference occurs for each FDM channel as described above, because the same multitone is used for each FDM channel, the NMSE in the presence of transceiver IQI can be derived as

$$\begin{aligned}\text{NMSE} \quad \approx \quad & |\alpha_{\rm r}\alpha_{\rm t} - 1|^2 + |\alpha_{\rm r}\beta_{\rm t}|^2 + \\ & |\beta_{\rm r}\beta_{\rm t}^*|^2 + |\beta_{\rm r}\alpha_{\rm t}|^2, \end{aligned} \tag{37}$$

where

$$\begin{aligned} \alpha_{\rm t} &= \tfrac{1+(1+\varepsilon_t)\exp(\mathrm{j}\theta_t)}{2}, \quad \beta_{\rm t} = \tfrac{1-(1+\varepsilon_t)\exp(\mathrm{j}\theta_t)}{2}, \\ \alpha_{\rm r} &= \tfrac{1+(1+\varepsilon_r)\exp(-\mathrm{j}\theta_r)}{2}, \quad \beta_{\rm r} = \tfrac{1-(1+\varepsilon_r)\exp(\mathrm{j}\theta_r)}{2}, \end{aligned} \tag{38}$$

and ε and θ denote IQI parameters of gain and phase difference, respectively, and subscripts t and r denote the transmitter and receiver, respectively. The derivation of (37) is shown in Appendix A. It is noted that if we assume that $\alpha_{\rm r} \approx 1, \beta_{\rm r} \approx 0$, (i.e., almost perfect receiver IQI compensation), then (37) can be approximately reduced to

$$\text{NMSE} \approx |\alpha_{\rm t} - 1|^2 + |\beta_{\rm t}|^2, \tag{39}$$

which is equal to twice the image rejection ratio (IRR), as shown in Appendices A and B.

To avoid the IQI effect in a simple way, this paper considers an alternative approach to multitone allocation by reducing the number of tones and offsetting the entire band. That is, the multitone allocation in (5) is modified with a reduced number of tones as

$$\bar{\bar{\Psi}}_{k'} = \begin{cases} \sqrt{M_{\rm d}}\bar{\Psi}_{k_2\sqrt{M_{\rm d}}} & \begin{array}{l}\mathrm{mod}(k', M_{\rm d}) = M_{\rm ofs}, \\ 0 \le k_2 < \frac{N}{2M_{\rm d}}\end{array} \\ \sqrt{M_{\rm d}}\bar{\Psi}_{\left(k_2 - \frac{N_f}{2M_{\rm d}}\right)\sqrt{M_{\rm d}}} & \begin{array}{l}\mathrm{mod}(k', M_{\rm d}) = M_{\rm ofs}, \\ \frac{N_f}{M_{\rm d}} - \frac{N}{2M_{\rm d}} \le k_2 < \frac{N_f}{M_{\rm d}}\end{array} \\ 0 & \text{otherwise} \end{cases} \tag{40}$$

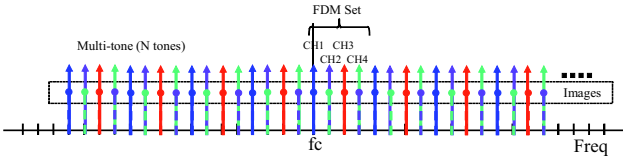

(a) Full-tone allocation.

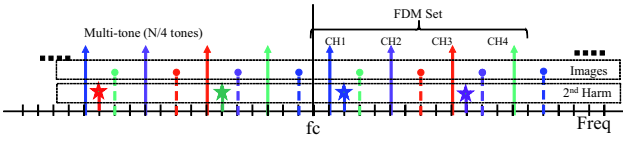

(b) Quarter-tone allocation.

Fig. 5. Passband spectra of two multitone allocation modes.

where $k_2 = \lfloor \frac{k'}{M_{\rm d}} \rfloor$ ($\lfloor g \rfloor$ denotes the greatest integer less than g), and $M_{\rm d}$ and $M_{\rm ofs}$ denote the reducing factor and the offset value from DC, respectively. For example, the quarter-tone allocation ($M_{\rm d} = 4$) with a single sub-carrier offset ($M_{\rm ofs} = 1$) in the same frequency resolution allows the image components' sub-carrier locations to be controlled, as shown in Fig. 5(b). As can be seen, the quarter-tone allocation induces the image components to appear only at the empty tone sub-carrier locations, so that the input tones are not interfered with by the mirror image component, though it will also be distorted by itself as in (45), in Appendix A.

Because the signal tones are not interfered with by the corresponding mirror image components, similar to the case of the IRR evaluation discussed in Appendices A and B, the k-th tone distorted by transceiver IQI in the quarter-tone allocation can be expressed as

$$\begin{aligned}&\tilde{Y}[k] = \\ &\quad (\alpha_{\rm r}\alpha_{\rm t}H[k] + \beta_{\rm r}\beta_{\rm t}^* H^*[N-k-1])\, S[k] + Z[k], \end{aligned} \tag{41}$$

where the tone index $N-k-1$ indicates the mirror frequency index of k if the set $\{H[0], ..., H[N/2-1]\}$ at the positive side and the set $\{H[N-1], ..., H[N/2]\}$ at the negative side are allocated symmetrically to the center frequency with an offset. We can see that the channel transfer function scaled by a constant $\alpha_{\rm r}\alpha_{\rm t}$ can be approximately obtained by dividing both sides of (41) by $S[k]$, because $|\beta_{\rm r}\beta_{\rm t}^*|$ usually yields a sufficiently small value. The physical meaning of the scaled transfer function is not changed from that of the original one; thus, it is seen that the quarter-tone allocation can greatly relax the requirement of the transceiver IQI compensation level, which is a very complicated and time-consuming task. The advantage of the quarter-tone allocation is deduced from the NMSE for the scaled channel transfer function, which is derived as

$$\text{NMSE}_{\rm scaled} = \frac{\sum_k \left|\hat{H}[k] - \alpha_{\rm r}\alpha_{\rm t}H[k]\right|^2}{\sum_k |\alpha_{\rm r}\alpha_{\rm t}H[k]|^2} = \frac{|\beta_{\rm r}\beta_{\rm t}^*|^2}{|\alpha_{\rm r}\alpha_{\rm t}|^2}, \tag{42}$$

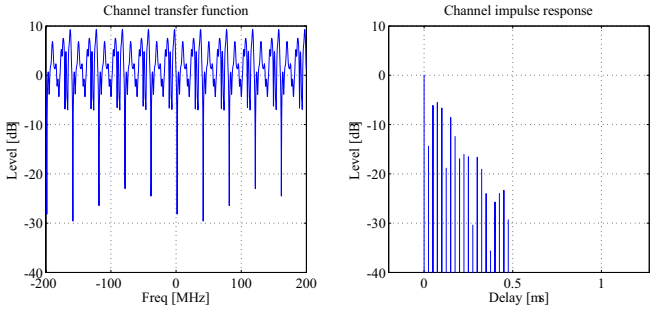

Fig. 6. Used channel model; the left and right figures show $H_{11}(f)$ and $h_{11}(\tau)$, respectively.

where

$$\hat{H}_{\text{scaled}}[k] = \alpha_{\text{r}}\alpha_{\text{t}}H[k] + \beta_{\text{r}}\beta_{\text{t}}^{*}H^{*}[N-k-1], \qquad (43)$$

which indicates the estimated channel transfer function in the quarter-tone scheme without noise. As discussed above, (42) becomes a much smaller value than (37) because $|\beta_{\text{r}}\beta_{\text{t}}^{*}|$ is usually very small. If there is no receiver IQI, (42) is simply reduced to zero.

Moreover, it is also robust to carrier leakage and the second-order harmonic components. It is noted that the sounding symbol in the quarter-tone allocation is shortened by $1/M_{\text{d}}$ and is repeated M_{d} times, which provides an additional gain in output SNR by M_{d}.

B. Phase Noise (PN) Effect

As is well documented in a rich literature, e.g., [20], [22], the phase noise of the local oscillator's PLL (phase lock loop) causes the inter-carrier interference (ICI) to distort the multi-carrier signals. PN, which is classified as a random noise effect, has also been mathematically modeled in many literatures, e.g., [21], [23]. Obviously, the multitone signals in the proposed channel sounding scheme are also significantly affected by the phase noise. Mitigation techniques for the PN effect have been intensively studied for multi-carrier data transmission.

Such techniques, however, cannot be applied for purposes of channel measurement due to the inseparability of the channel and the hardware effects. Therefore a high-precision PLL is required in order to accurately measure the channel transfer functions within a relatively long symbol duration as compared with the phase drift caused by the PN, and to measure the dynamic channel properties such as Doppler characteristics from consecutively measured snapshots.

V. Evaluation of Measurement Accuracy

In this section, the NMSE performance of the channel measurement accuracy in the presence of impairments of the RF front-end is analyzed by Monte Carlo simulation.

A. Simulation Parameters

Table I presents the simulation parameters based on the specifications of the MIMO channel sounder, which has been developed to characterize the radio channel property for future MIMO cellular systems beyond IMT-Advanced. To realize data transmission throughput above 30 Gbps, a further increase in frequency bandwidth is crucial, in addition to the number of spatially multiplexed streams in MIMO OFDM transmission, where we assume a wide bandwidth of 400 MHz at 11 GHz as a new candidate frequency that is higher than 5 GHz and with up to a 24×24 MIMO configuration.

TABLE I
Simulation parameters.

Unit configuration	
No. Tx units (N_{Utx})	1, 2, 3, and 6
No. Rx units (N_{Urx})	1, 2, 3, and 6
No. antennas per unit (N_A)	4
Multitone signal	
Carrier frequency	11 GHz
Signal bandwidth ($2B$)	400 MHz
Sampling rates (f_s)	800 MHz (R_{ov}=2)
No. tones (N)	$2,048$
Tone spacing (Δ_F)	195 kHz
Fundamental symbol duration	5.12 μs
FFT length (N_f)	$4,096$
GI length (N_{GI})	800
FDM	
FDM channels (L)	N_A
FDM tone spacing (Δ_f)	48.8 kHz
FDM FFT duration	20.48 μs ($= LN_f/2B$)
FDM GI duration	4 μs ($= LN_{\text{GI}}/2B$)
FDM symbol duration (T_{FDM})	24.48 μs
STDM	
STDM channels	N_{Utx}
Beamforming weight	DFT beam
STDM symbol duration (T_{STDM})	24.48, 48.96, 73.44, and 146.88 μs
Channel model	Rayleigh fading 20-path exponential power decay, delay spread = 0.5μs

The number of tones in the multitone signal is $2,048$ over the signal bandwidth; thus, the tone spacing is 195 KHz. The tone spacing of a 4-channel FDM is reduced by a quarter (48.8 KHz), and the FDM symbol duration is 24.48 μs, consisting of FFT (20.48 μs) and GI (4 μs) durations which are 4 times the values of the fundamental multitone signal.

In this paper, a widely accepted channel model is used to evaluate the estimation accuracy of the channel transfer function in the presence of transceiver imperfections. In our simulations, an i.i.d. MIMO channel was generated by a Rayleigh fading model with an exponentially decaying power delay profile of $\rho^{-d/(N_{\text{path}}-1)}$, where $d = 0, ..., N_{\text{path}} - 1$ and ρ denotes the power ratio of the first and last path. Here, $N_{\text{path}} = 20$, $\rho = 30$ dB, and the delay spacing was 10 samples (The maximum delay spread is 0.5 μs, which was empirically chosen in the measurement at 11 GHz.) For each path, Rayleigh fading was generated by adding 5 ray components with equal power but random phases. It is also assumed that the channel responses are static during the measurement, i.e., the Doppler frequency was neglected. The generated channel transfer function and impulse response are shown in Fig. 6.

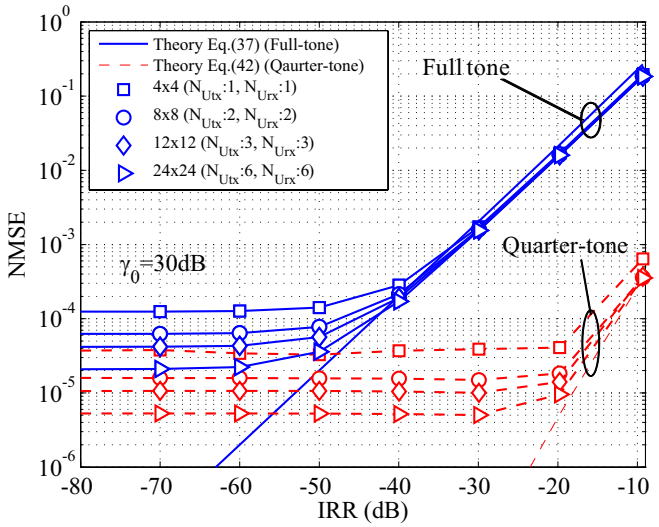

Fig. 7. Transceiver IQI effect on the channel measurement accuracy in proposed scalable architecture ($\gamma_0 = 30$ dB).

TABLE II
PHASE NOISE MODELS.

[dBc/Hz]	1 kHz	10 kHz	100 kHz	1 MHz	10 MHz
Model 1 (normal)	−62	−68	−97	−120	−140
Model 2 (high-precision)	−103	−112	−117	−133	−140

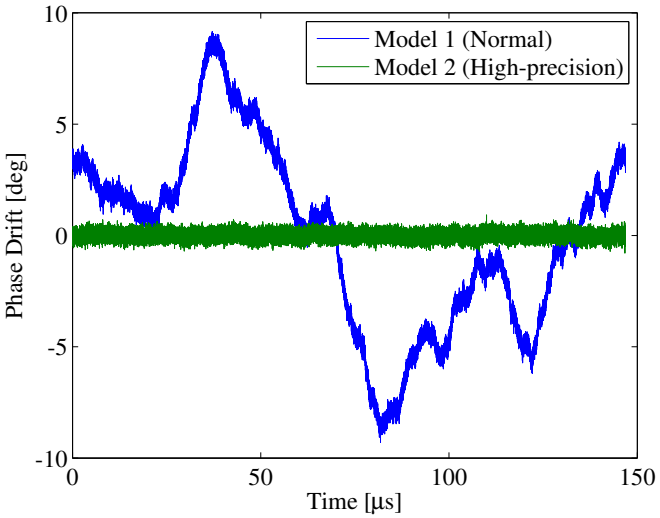

(a) Temporal phase drift due to the phase noise between the LOs in transmitter and receiver (randomly generated based on the models of Table. II).

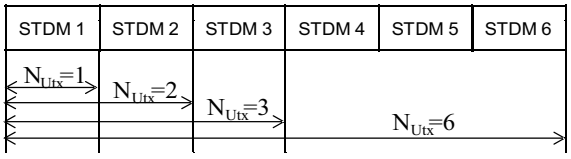

(b) Scalable measurement duration.

Fig. 8. Temporal phase drift for 146.88 μs (measurement duration in case of $N_{\mathrm{Utx}} = 6$) and scalable measurement durations.

B. Performance Bound and Processing Gain

It is obvious that the NMSE will decrease with an increase in γ_0, the average SNR per transmit antenna if there are no other imperfections. As described in (36) in Section II, the proposed scheme basically has multiplexing gains (G_{mux}) in the output SNR; thus, the NMSE along with γ_0 will decrease to a much greater degree than in the conventional TDM transmitter switching scheme, thanks to the simultaneous multiple transmission, which transmits as many times as the total number of transmit antennas ($N_{\mathrm{T}} = LN_{\mathrm{Utx}}$). Each transmit signal can be separated by FDM and STDM signal processing at both the transmitters and receivers, where the multiplexing gain in an output SNR of

$$G_{\mathrm{mux}}[\mathrm{dB}] = 10\log_{10} L + 10\log_{10} N_{\mathrm{Utx}} \tag{44}$$

can be achieved. It is noted that the transmitting power per antenna is assumed to be the same in both cases of single and multiple transmit antennas.

If over-sampling in ADCs at a rate of R_{ov} is considered in an actual implementation, an additional gain of $10\log_{10} R_{\mathrm{ov}}$ dB can be achieved by discarding the noise component at the upper band and extracting only the tones in the lower band in the frequency domain. Finally, the gain produced by the quarter-tone allocation yields $10\log_{10} M_{\mathrm{d}}$ dB. Therefore, in a 24×24 MIMO configuration where $N_{\mathrm{Utx}} = N_{\mathrm{Urx}} = 6$ and $L = 4$, the processing gains for full-tone allocation and quarter-tone allocation are approximately 17 and 23 dB in all, respectively.

C. Effects of I/Q imbalance and Phase Noise

1) I/Q imbalance: As a combined effect of the phase imbalance and relative amplitude difference (θ and ε), consider the power ratio of the image component to the signal, namely, IRR [17]–[19]. Fig. 7 shows the transceiver IQI effects on the channel measurement accuracy for various scalable unit configurations that were evaluated in terms of an IRR level with $\gamma_0 = 30$ dB, where IRR includes both the transmitter and receiver IQIs. In full-tone allocation, it is seen that the NMSE linearly decreases along with a decrease in IRR when IRR is large, and approaches the ideal value for a given SNR with a gain of the number of transmitter units (N_{Utx}) in (36). The NMSE is almost twice the IRR when the receiver IRR is small (to be exact, both IRRs at the transmitter and receiver are small in this simulation), as discussed in Section IV-A. It is seen that the NMSE was not influenced by increasing the number of units in a large IRR (when the IRR is dominant over the noise effect), because the IQI generates only self- and inter-channel interference between the FDM channels. From the results, it can also be seen that a NMSE of approximately 2.0×10^{-4} (EVM is equivalently 1.4 %) can be achieved if the IRR levels at both the transmitter and receiver are compensated for below -40 dB.

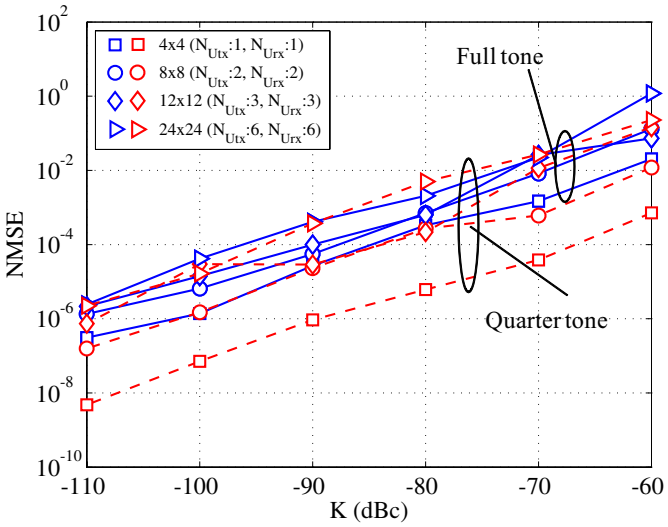

Fig. 9. Phase noise effect on the channel measurement accuracy in proposed scalable architecture (without noise).

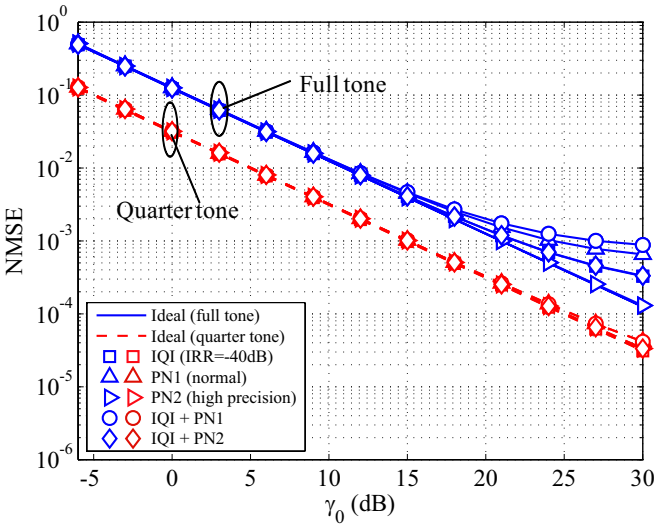

(a) 4×4 MIMO ($N_{\mathrm{Utx}} = N_{\mathrm{Urx}} = 1$).

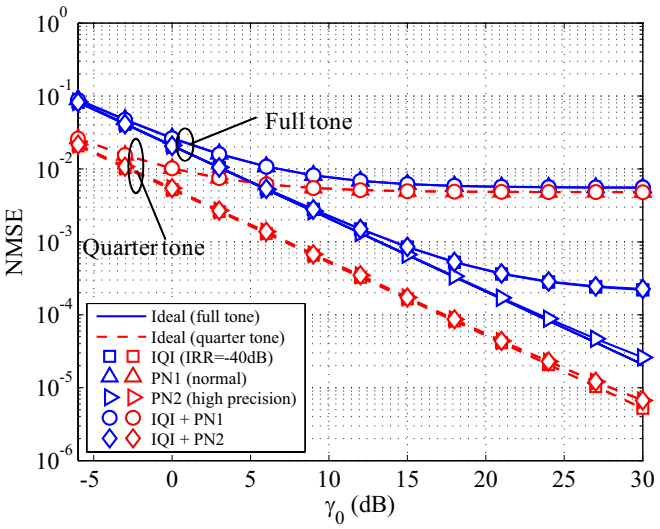

(b) 24×24 MIMO ($N_{\mathrm{Utx}} = N_{\mathrm{Urx}} = 6$).

Fig. 10. NMSE performance with transceiver imperfections where IRR = -40 dB.

On the other hand, the quarter-tone allocation shows good robustness against the IQI effect because the NMSEs have almost ideal values for a given SNR until an IRR of around -30 dB where the constant distortion (i.e., $\alpha_{\mathrm{t}}\alpha_{\mathrm{r}}$ in (42)) across the signal bandwidth due to the IQI were ignored and were not included into the NMSE calculation. As can be seen from the results, the quarter-tone allocation scheme still suffers from the receiver IQI, though it can perfectly mitigate the transmitter IQI. However, it can also be seen that the receiver IQI causes interference from the image of the image component; thus, it is usually not very significant up to IRR=-30 dB, at which point the power of the image component is usually negligible.

2) Phase Noise: Next, the phase noise effects on the channel measurement accuracy were evaluated in various scalable unit configurations. In the simulations, the temporal phase drift due to the phase noise effect was generated by filtering the Gaussian noise with the spectrum shape of the model presented in Table II, in which two phase noise models corresponding to normal and high-precision PLLs are specified. Fig. 8 shows an example of phase drifts for 146.88 μs (measurement duration in $N_{\mathrm{Utx}} = 6$ ($N_{\mathrm{T}} = 24$) configuration) that are randomly generated based on these models. Fig. 9 shows the NMSEs without noise in terms of the peak value K at 1 KHz, where the spectrum shape of Model 1 was used. It is seen that the NMSE performance was degraded as the number of units increased, because the symbol duration of FDM-STDM became lengthened such that it was strongly affected by long-term phase rotation, as shown in Fig. 8(b). It is noted that this simulation assumed that one LO is used commonly in all transmitter units, and another LO is used commonly in all receiver units, respectively; thus, all pairs of transmitter and receiver units are affected by an identical phase noise effect. However the results become worse if each unit has a different LO, because each STDM symbol is affected by an independent phase drift. In the quarter-tone allocation, it is noted that the short symbol duration (large sub-carrier spacing) in the 4×4 MIMO configuration results in noticeably better NMSE than other configurations.

D. Measurement Accuracy with Transceiver Imperfections

To gain insight into the degree of measurement accuracy under more practical conditions, NMSEs in the presence of transceiver impairments of IQI (IRR=-40 dB at both the transmitter and the receiver) and PN (Models 1 and 2) were evaluated in terms of the average SNR per transmit antenna (γ_0). Figs 10(a) and 10(b) show the NMSEs in 4×4 and 24×24 MIMO configurations, respectively. As can be seen from both sets of results, the phase noise effect is a critical factor in the channel measurement accuracy according to the

measurement duration, where we assume that the receiver IQI is reasonably compensated for by an IRR of -40 dB. Moreover, the IQI effect is not significant because the noise is quite dominant during evaluation of the performance up to a SNR of 30 dB. We can see in Fig. 10(b) that in the presence of IQI and PN (Model 1), the NMSEs in 4×4 and 24×24 are not improved even with a SNR larger than 30 dB, which are below around 0.001 and 0.006 and roughly corresponds to EVMs of around 3.16% and 7.75%, respectively. On the other hand, the PN effect is almost perfectly mitigated by the use of high-precision PLL in both results. As regards only PN, as expected, the NMSEs in the 24×24 configuration are much more degraded than those in the 4×4 configuration due to its long measurement duration. Finally, it is seen that the IQI effect is completely removed in the quarter-tone allocation.

VI. Conclusion and Remarks

This paper has presented a new concept of a scalable MIMO channel sounding technique with parallel transceiver architecture, in which a layered scheme of FDM and STDM is employed for both the directional MIMO channel and multi-link MIMO channel measurements. In this technique, a quarter-tone allocation scheme was developed in order to efficiently mitigate IQI effects. Moreover, from a channel sounding point of view, the design and implementation issues were comprehensively discussed. Using computer simulations, the channel measurement accuracy in the presence of two critical impairments of RF front-ends, I/Q imbalance and phase noise was evaluated using NMSE. From the quantitative evaluation results, it was seen that IQI can be completely mitigated by the quarter-tone allocation, and a high-precision PLL is necessary to reduce the phase noise effect sufficiently.

Using the proposed technique, we have initially developed the basic configuration with a 4×4 MIMO system [10], i.e., $L = 4$ and $N_{\mathrm{Utx}} = N_{\mathrm{Urx}} = 1$, and it has been extended by a 24×24 MIMO configuration where $N_{\mathrm{Utx}} = 6$ and $N_{\mathrm{Urx}} = 6$. The aim of the study is to achieve wideband radio channel characterization with a bandwidth of 400 MHz at 11 GHz in various measurement scenarios, and it has been conducted as a fundamental study for the next generation wireless mobile communication systems.

Acknowledgment

This work was partly supported by "The research and development project for expansion of radio spectrum resources" of The Ministry of Internal Affairs and Communications, Japan. The authors would like to express the appreciation to Professors H. Suzuki, K. Fukawa and S. Suyama of Tokyo Institute of Technology for their helpful discussions.

Appendix A
NMSE for Transceiver I/Q Imbalance (SISO)

Assuming a frequency-independent IQI at both the transmitter and receiver, we consider the k-th probing tone (N tones in all), as discussed in Section III-A. The tone distorted by the quadrature modulator's IQI at the transmitter [17], [19] can be expressed as

$$\tilde{S}[k] = \alpha_{\mathrm{t}} S[k] + \beta_{\mathrm{t}} S^*[N-k-1]. \tag{45}$$

The tone index $N-k-1$ indicates the mirror frequency index of k if the tones $\{S[0], ..., S[N/2-1]\}$ at the positive side and the tones $\{S[N-1], ..., S[N/2]\}$ at the negative side are allocated symmetrically to the center frequency.

Similarly, the signal that is received through the channel is distorted again by the quadrature demodulator's IQI at the receiver can be expressed as

$$\begin{aligned}\tilde{Y}[k] = \alpha_{\mathrm{r}} H[k] \tilde{S}[k] + \\ \beta_{\mathrm{r}} H^*[N-k-1] \tilde{S}^*[N-k-1] + Z[k].\end{aligned} \tag{46}$$

Using (30), the estimated channel transfer function distorted by transceiver IQI is written as

$$\hat{H}[k] = \eta_1[k] H[k] + \eta_2[k] H^*[N-k-1] + Z[k] S^{-1}[k], \tag{47}$$

where

$$\eta_1[k] = \alpha_{\mathrm{r}}\alpha_{\mathrm{t}} + \alpha_{\mathrm{r}}\beta_{\mathrm{t}} S^*[N-k-1] S^{-1}[k], \tag{48}$$

$$\eta_2[k] = \beta_{\mathrm{r}}\beta_{\mathrm{t}}^* + \beta_{\mathrm{r}}\alpha_{\mathrm{t}}^* S^*[N-k-1] S^{-1}[k], \tag{49}$$

and we assume that $T[k]R[k] = 1, \forall k$. Then, assuming that $\frac{1}{N}\sum_{k=0}^{N-1} |H[k]|^2 = 1$, the NMSE for the transceiver IQI can be simply derived as

$$\begin{aligned}\mathrm{NMSE} &= \frac{1}{N}\sum_{k=0}^{N-1} \Big| \left(\eta_1[k] - 1\right) H[k] + \\ &\qquad \eta_2[k] H^*[N-k-1] + Z[k] S^{-1}[k] \Big|^2 \qquad (50) \\ &\approx \frac{1}{N}\sum_{k=0}^{N-1} \Big(\left|\eta_1[k] - 1\right|^2 \left|H[k]\right|^2 + \\ &\qquad \left|\eta_2[k]\right|^2 \left|H^*[N-k-1]\right|^2 \Big) \qquad (51)\end{aligned}$$

where the approximation of (51) can be made when $\sum_{k=0}^{N-1} H[k] H^*[N-k-1] = 0$ (the channel transfer functions at any frequency k and the mirror frequency $N-k-1$ are uncorrelated) and the SNR is large enough. By replacing NPM Ψ_k with $S[k]$, (51) can be further approximated as

$$\begin{aligned}\mathrm{NMSE} \approx |\alpha_{\mathrm{r}}\alpha_{\mathrm{t}} - 1|^2 + |\alpha_{\mathrm{r}}\beta_{\mathrm{t}}|^2 + \\ |\beta_{\mathrm{r}}\beta_{\mathrm{t}}^*|^2 + |\beta_{\mathrm{r}}\alpha_{\mathrm{t}}|^2 + \Omega + \Omega^*,\end{aligned} \tag{52}$$

where

$$\Omega = \frac{1}{N}\sum_{k=0}^{N-1} \left(|H[k]|^2 + |H[N-k-1]|^2 \right) \Psi_k \Psi_{k+1} \tag{53}$$

which usually yields very small value if the power sum of the channel transfer functions at frequencies that mutually mirror one another can be regarded as being approximately constant, since $\frac{1}{N}\sum_{k=0}^{N-1} \Psi_k \Psi_{k+1} \approx 0$.

On the other hand, the image rejection ratio (IRR) as measured by a single tone input $S[k]$ (without a mirror frequency

tone, i.e., $S[N-k-1]=0$) is calculated by

$$\begin{aligned}\text{IRR} &= \frac{\sum_k |\tilde{Y}[k]-Y_0[k]|^2}{\sum_k |Y_0[k]|^2} && (54)\\ &= \frac{1}{N}\sum_{k=0}^{N-1}\Big|(\alpha_{\rm r}\alpha_{\rm t}-1)H[k]+ \\ &\quad \beta_{\rm r}\beta_{\rm t}^* H^*[N-k-1]+Z[k]S^{-1}[k]\Big|^2 && (55)\\ &\approx \Big|\alpha_{\rm r}\alpha_{\rm t}-1\Big|^2+\Big|\beta_{\rm r}\beta_{\rm t}^*\Big|^2 && (56)\end{aligned}$$

where

$$\begin{aligned}Y_0[k] &= H[k]S[k], && (57)\\ \tilde{Y}[k] &= (\alpha_{\rm r}\alpha_{\rm t}H[k]+\beta_{\rm r}\beta_{\rm t}^*H^*[N-k-1])\,S[k] \\ &\quad +Z[k]. && (58)\end{aligned}$$

In (56), the approximation can be made because the product of $(\alpha_{\rm r}\alpha_{\rm t}-1)$ and $\beta_{\rm r}\beta_{\rm t}^*$ usually yields a very small value. Finally, it is seen that the NMSE in (52) is approximately twice the IRR in (56) when the receiver IQI effect is small enough, that is, $\alpha_{\rm r}\approx 1$ and $\beta_{\rm r}\approx 0$.

APPENDIX B
NMSE FOR TRANSCEIVER I/Q IMBALANCE (MIMO)

Consider the NMSE for the case of MIMO in which, for the sake of simplicity, the IQI parameters for each pair of transmitters and receivers are identical for all MIMO channels. Similar to the case in Appendix A, if we assume that $\frac{1}{N_{\rm Utx}N_{\rm R}N}\sum_{k=0}^{N-1}\|\boldsymbol{H}^{((l))}[k]\|_{\rm F}^2=1$, the NMSE in MIMO can be represented by averaging those for each FDM channel as

$$\text{NMSE}=\frac{1}{L}\sum_{l=1}^{L}\text{NMSE}^{((l))} \quad (59)$$

where

$$\begin{aligned}&\text{NMSE}^{((1))}= \\ &\frac{1}{N_{\rm Utx}N_{\rm R}N}\sum_{k=0}^{N-1}\Bigg(\Big\|\left(\eta_1^{((1))}[k]-1\right)\boldsymbol{H}^{((l))}[k] \\ &\quad +\eta_2^{((1))}[k]\boldsymbol{H}^{((1))}[N-k] \\ &\quad +\boldsymbol{Z}^{((1))}[k]\left(\boldsymbol{X}^{((1))}[k]\right)^{-1}\Big\|_{\rm F}^2\Bigg), \quad (60)\end{aligned}$$

$$\begin{aligned}&\text{NMSE}^{((2))}+\text{NMSE}^{((4))}= \\ &\frac{1}{N_{\rm Utx}N_{\rm R}N}\Bigg(\sum_{k=0}^{N-1}\Bigg(\Big\|\left(\eta_1^{((2))}[k]-1\right)\boldsymbol{H}^{((2))}[k] \\ &\quad +\eta_2^{((4))}[k]\boldsymbol{H}^{((4))}[N-k-1] \\ &\quad +\boldsymbol{Z}^{((2))}[k]\left(\boldsymbol{X}^{((2))}[k]\right)^{-1}\Big\|_{\rm F}^2\Bigg) \\ &\quad +\sum_{k=0}^{N-1}\Bigg(\Big\|\left(\eta_1^{((4))}[k]-1\right)\boldsymbol{H}^{((4))}[k] \\ &\quad +\eta_2^{((2))}[k]\boldsymbol{H}^{((2))}[N-k-1] \\ &\quad +\boldsymbol{Z}^{((4))}[k]\left(\boldsymbol{X}^{((4))}[k]\right)^{-1}\Big\|_{\rm F}^2\Bigg)\Bigg) \quad (61)\end{aligned}$$

and

$$\begin{aligned}&\text{NMSE}^{((3))}= \\ &\frac{1}{N_{\rm Utx}N_{\rm R}N}\sum_{k=0}^{N-1}\Bigg(\Big\|\left(\eta_1^{((3))}[k]-1\right)\boldsymbol{H}^{((3))}[k] \\ &\quad +\eta_2^{((3))}[k]\boldsymbol{H}^{((3))}[N-k-1] \\ &\quad +\boldsymbol{Z}^{((3))}[k]\left(\boldsymbol{X}^{((3))}[k]\right)^{-1}\Big\|_{\rm F}^2\Bigg). \quad (62)\end{aligned}$$

where

$$\eta_1^{((l))}[k] = \begin{cases}\alpha_{\rm r}\alpha_{\rm t}+\alpha_{\rm r}\beta_{\rm t}\Psi_k^*\Psi_k^* & l=1\\ \alpha_{\rm r}\alpha_{\rm t}+\alpha_{\rm r}\beta_{\rm t}\Psi_k^*\Psi_{k+1}^* & \text{otherwise}\end{cases}, \quad (63)$$

$$\eta_2^{((l))}[k] = \begin{cases}\beta_{\rm r}\beta_{\rm t}^*+\beta_{\rm r}\alpha_{\rm t}^*\Psi_k^*\Psi_k^* & l=1\\ \beta_{\rm r}\beta_{\rm t}^*+\beta_{\rm r}\alpha_{\rm t}^*\Psi_k^*\Psi_{k+1}^* & \text{otherwise}\end{cases}. \quad (64)$$

From the fact that the tone allocation in FDM CH 1 uses DC (the center frequency in passband), it is noted that its interference pattern differs from that of the other FDM channels, and that FDM CH2 and CH4 interfere with each other; thus, the NMSE should be expressed in a merged form of the two. Further, if we assume that the individual MIMO channels are statistically independent and identically distributed and SNR is large enough, then (59) can be approximately rewritten as

$$\begin{aligned}\text{NMSE} &\approx |\alpha_{\rm r}\alpha_{\rm t}-1|^2+|\alpha_{\rm r}\beta_{\rm t}|^2+ \\ &\quad |\beta_{\rm r}\beta_{\rm t}^*|^2+|\beta_{\rm r}\alpha_{\rm t}|^2. \quad (65)\end{aligned}$$

Moreover, the IRR for the MIMO case is also identical to (56) as

$$\text{IRR} \approx \Big|\alpha_{\rm r}\alpha_{\rm t}-1\Big|^2+\Big|\beta_{\rm r}\beta_{\rm t}^*\Big|^2. \quad (66)$$

REFERENCES

[1] V. Kolmonen, P. Almers, J. Salmi, J. Koivunen, K. Haneda, A. Richter, F. Tufvesson, A. F. Molisch, and P. Vainikainen, "A Dynamic Dual-Link Wideband MIMO Channel Sounder for 5.3 GHz," *IEEE Trans. Instrum. Meas.*, vol. 59, no. 4, pp. 873–883, Apr. 2010.

[2] J. Poutanen, F. Tufvesson, K. Haneda, V. Kolmonen, and P. Vainikainen, "Multi-Link MIMO Channel Modeling Using Geometry-Based Approach," *IEEE Trans. Antenna Propag.*, vol. 60, no. 2, pp. 587–596, Apr. 2012.

[3] N. Czink, "Empirical investigation of multi-link separation for indoor MIMO channels," Proc. *IEEE Symposium on Personal, Indoor and Mobile Radio Communications (PIMRC)*, Sept. 2011.

[4] C. Oestges and N. Czink, "Analytical Multi-User MIMO Channel Modeling: Subspace Alignment Matters," *IEEE Trans. Wireless Commnun.*, vol. 11, no. 1, pp. 367–377, Nov. 2011.

[5] RUSK Channel Sounder, MEDAV, http://www.channelsounder.de/

[6] G. Gutierrez, O. Gonzalez, J. Perez, D. Ramirez, L. Vielva, J. Ibanez, I. Santamaria, "Frequency-Domain Methodology for Measuring MIMO Channels Using a Generic Test Bed," *IEEE Trans. Instrum. Meas.*, vol. 60, no. 3, pp. 827–837, Mar. 2011.

[7] B. Maharaj, J. Wallace, M. Jensen and L. Linde, "A Low-Cost Open-Hardware Wideband Multiple-Input-Multiple-Output (MIMO) Wireless Channel Sounder," *IEEE Trans. Antenna Propag.*, vol. 57, no. 10, pp. 2285–2289, Oct. 2008.

[8] V. Kolmonen, J. Kivinen, L. Vuokko, and P. Vainikainen, "5.3-GHz MIMO Radio Channel Sounder," *IEEE Trans. Instrum. Meas.*, vol. 55, no. 4, pp. 1263–1269, Aug. 2006

[9] K. Sakaguchi, J. Takada, and K. Araki, "A novel architecture for MIMO spatio-temporal channel sounder," *IEICE Trans. Electron.*, vol. 85, no. 3, pp. 436–441, 2002.

[10] Y. Konishi, M. Kim, M. Ghoraishi, J. Takada, S. Suyama and H. Suzuki, "Channel Sounding Technique using MIMO Software Radio Architecture," Proc. *the 5th European Conference on Antennas and Propagation (EuCAP)*, Rome, Italy, Apr. 2011.

[11] R. Pirkl and G. Durgin, "Optimal Sliding Correlator Channel Sounder Design," *IEEE Trans. Wireless Commun.*, vol. 7, no. 9, pp. 3488–3497, Sept. 2008.

[12] M. Kim, H. You and H. Lee, "A Novel Transmit Scheme in CDM-based MIMO Channel Sounding Systems," *IEICE Trans. Commun.*, vol. E93, no. 9, pp. 2428–2432, Sept. 2010.

[13] D. Laurenson and P. Grant, "A Review of Radio Channel Sounding Techniques," in Proc. *European Signal Processing Conference (EUSIPCO)*, Florence, Italy, Sept. 2006.

[14] G Fettweis, M Lohning, D. Petrovic, M. Windisch, P. Zillmann, and W. Rave, "Dirty RF: A New Paradigm," Proc. *IEEE Symposium on Personal, Indoor and Mobile Radio Communications (PIMRC)*, Sept. 2005.

[15] M. Valkama, M. Renfors and V. Koivunen, "Advanced methods for IQ imbalance compensation in communication receivers," *IEEE Trans. Signal Processing*, vol. 49, no. 10, pp. 2335–2344, Oct. 2001.

[16] O. Myllari, L. Anttila and M. Valkama, "Digital Transmitter I/Q Imbalance Calibration: Real-Time Prototype Implementation and Performance Measurement", Proc. *EURSIPCO*, pp. 537–541, Aug. 2010.

[17] L. Anttila, M. Valkama and M. Renfors, "Frequency-Selective I/Q Mismatch Calibration of Wideband Direct-Conversion Transmitters", *IEEE Trans. Circuits Syst. II*, vol. 55, no. 4, pp. 359–363, Apr. 2008.

[18] M. Kim, Y. Konishi, J. Takada and B. Gao, "Automatic IQ Imbalance Compensation Technique for Quadrature Modulator by Signle-Tone Testing," *IEICE Trans. Commun.* vol. E95-B, no. 5, pp.1864–1868, May. 2012.

[19] D. Tandur and M. Moonen, "Joint Compensation of OFDM Frequency-Selective Transmitter and Receiver IQ Imbalance," *EURASIP J. Wireless Commun. Networking*, vol 2007, Article ID 68563, 2007.

[20] S. Suyama, H. Suzuki, K. Fukawa and J. Izumi, "Iterative Receiver Employing Phase Noise Compensation and Channel Estimation for Millimeter-Wave OFDM Systems," *IEEE J. Select. Areas Commun.*, vol. 27, no. 8, pp. 1357–1366, Oct. 2009.

[21] A. Taparugssanagorn and J. Ylitalo, "Characteristics of Short-Term Phase Noise of MIMO Channel Sounding and Its Effect on Capacity Estimation," *IEEE Trans. Instrum. Meas.*, vol. 58, no. 1, pp. 196–201, Jan. 2009.

[22] D. Petrovic, W. Rave, and G. Fettweis, "Effects of phase noise on OFDM systems with and without PLL: characterization and compensation," *IEEE Trans. Commun.*, vol. 55, no. 8, pp. 1607–1616, Aug. 2007.

[23] D. Baum and H. Bolcskei, "Impact of Phase Noise on MIMO Channel Measurement Accuracy," Proc. *2004 IEEE Vehicular Technology Conf. (VTC)*, Sept. 2004.

[24] S. Salous, R. Lewenz, I. Hawkins, N. Razavi-Ghods and M. Abdallah, "Parallel receiver channel sounder for spatial and MIMO characterisation of the mobile radiochannel," *Proc. IEE Commun.*, vol. 152, no. 6, pp. 912–918, Dec. 2005.

[25] K. Mizutani, K Sakaguchi, J. Takada, and K. Araki, "Development of MIMO-SDR Platform and Its Application to Real-Time Channel Measurements," *IEICE Trans. Commun.*, vol. E89-B, no. 12, pp. 3197–3207, Dec. 2006.

[26] S. Boyd, "Multitone signals with low crest factor," *IEEE Trans. Circuits Syst.*, vol. 33, no. 10, pp. 1018–1022, Oct. 1986.

[27] H. Arslan and H. Mahmoud, "Error vector magnitude to SNR conversion for nondata-aided receivers," *IEEE Trans. Wireless Commun.*, vol. 8, no. 5, pp. 2694–2704, May 2009.

Minseok Kim (S'02–M'05) was born in Seoul, Korea. He received the B.S. degree in Electrical Engineering from Hanyang University, Seoul, Korea, M.E. and D.E. degrees in Division of Electrical and Computer Engineering, Yokohama National University (YNU), Japan in 1999, 2002 and 2005, respectively. He has been with Tokyo Institute of Technology from 2007 as an assistant professor. He has been on leave to Georgia Institute of Technology as a visiting scholar in 2010.

His research interests include radio propagation channel measurement and modeling, body area network, antenna array signal processing, DSP implementation on FPGAs, cognitive and software defined radios. He received the Young Researcher's Encouragement Award of IEEE VTS Japan in 2003. He is a member of IEICE.

Jun-ichi Takada (S'89–M'93–SM'11) received B.E. and D.E. degrees from Tokyo Institute of Technology (Tokyo Tech), Japan, in 1987 and 1992, respectively. He was a Research Associate at Chiba University from 1992 to 1994, and an Associate Professor at Tokyo Tech from 1994 to 2006 where he has been a Professor since 2006. From 2003 to 2007, he was also a Researcher at the National Institute of Information and Communications Technology (NICT), Japan.

From 2007 to 2010, he was a co-chair of special interest group (SIG) E on "Body Communications" within EU COST Action 2100. His current interests include the radiowave propagation and channel modeling for various wireless systems, and regulatory issues of spectrum sharing. He received the achievement award of IEICE in 2008. He is a senior member of IEICE.

Yohei Konishi (S'08) received the B.E. degree in communication engineering from National Defense Academy, Japan, in 2005, and the M.E. degree in electrical and electronic engineering from Tokyo Institute of Technology, Japan, in 2009. He is currently working toward the D.E. degree at Tokyo Institute of Technology.

His research interests include MIMO channel sounding and modeling. He is a student member of IEICE.